Prediction of the Flow Around an Airfoil Using a Reynolds Stress Transport Model

Lars Davidson
Thermo and Fluid Dynamics,
Chalmers University of Technology,
S-412 96 Gothenburg, Sweden

A second-moment Reynolds Stress Transport Model (RSTM) is used in the present work for computing the flow around a two-dimensional airfoil. An incompressible SIMPLEC code is used, employing a non-staggered grid arrangement. A third-order QUICK scheme is used for the momentum equations, and a second-order, bounded MUSCL scheme is used for the turbulent quantities. As the RSTM is valid only for fully turbulent flow, an eddy viscosity, one-equation model is used near the wall. The two models are matched along a preselected grid line in the fully turbulent region. Detailed comparisons between calculations and experiments are presented for an angle of attack of $\alpha = 13.3$ deg. The RSTM predictions agree well with the experiments, and approaching stall is predicted for $\alpha = 17$ deg, which agrees well with experimental data. The results obtained with a two-layer $k - \epsilon$ model show poor agreement with experimental data; the velocity profiles on the suction side of the airfoil show no tendency of separation, and no tendency of stall is predicted.

Introduction

Flow around airfoils is an interesting turbulent flow configuration involving a number of fundamental physical flow phenomena such as transition, curvature-induced production of turbulence, separation and wake flow. Transition is usually not predicted but is prescribed from experimental data. Some work has been presented in which transition is predicted using the e^n-method based on the linearized stability theory (Cebeci, 1989). In real (industrial) configurations, it is of utmost importance to be able to predict the locations of transition; in the present study, however, the locations of transition are prescribed from experimental data.

Curvature effects, related either to curvature of the wall or streamline curvature, are known to have significant effects on the turbulence (Bradshaw, 1973). Both types of curvature are present in airfoil flows, the former on the suction side and the latter in and near the separation region. The entire Reynolds tensor is active in the interaction process between shear stresses, normal stresses and mean velocity strains. When predicting flows where curvature effects are important, it is thus necessary to use turbulence models that accurately predict all Reynolds stresses, not only the shear stresses.

Second-moment closures such as RSTM are superior to simpler turbulence models such as the $k - \epsilon$ or the Baldwin-Lomax models. The main reasons for their superiority are their ability to account for (i) streamline curvature, (ii) strong nonlocal effects and history effects for the individual stresses, and (iii) irrotational strains, phenomena which all are present in airfoil flow.

Contributed by the Fluids Engineering Division for publication in the JOURNAL OF FLUIDS ENGINEERING. Manuscript received by the Fluids Engineering Division March 23, 1993; revised manuscript received April 25, 1994. Associate Technical Editor: O. Baysal.

(i) When the streamlines in boundary layer type of flow have a convex (concave) curvature, the turbulence is stabilised (destabilized), which dampens (augments) the turbulence (Bradshaw, 1973; Rodi and Scheuerer, 1983), especially the shear stress and the Reynolds stress normal to the wall. Bradshaw demonstrates that even small amounts of convex curvature can have a significant effect on the turbulence. In the present configuration, both wall curvature and streamline curvature are present.

(ii) The adverse pressure gradient on the suction side of the airfoil with a subsequent separation produces strong anisotropy in the Reynolds stresses, which is transported downstream.

(iii) In boundary layer flow, the only term which contributes to the production term in the k equation is $-\rho\overline{uv}\partial U/\partial y$ (x denotes streamwise direction). Thompson and Whitelaw (1985) found that, near the separation point as well as in the separation zone, the production term $-\rho(\overline{u^2} - \overline{v^2})\partial U/\partial x$ is of equal importance. This is also the case for airfoil flow, where large irrotational strains ($\partial U/\partial x$, $\partial V/\partial y$) prevail, for example, near the point of separation.

In a previous paper (Davidson and Rizzi, 1992), an Algebraic Stress Model was applied on the same configuration as in the present study. In the ASM, which is a truncated form of the RSTM, the transport terms (convection and diffusion) are approximated as being proportional to the transport of turbulent kinetic energy. This is maybe a sound approximation for the normal stresses, but not for the shear stresses. The RSTM is superior to ASM, mainly because the more accurate treatment of convection and diffusion, where in the RSTM the individual stresses are transported independently of each other.

The paper is organized as follows: the mean flow equations are presented first, together with some details on the compu-

tational method. The turbulence model is described in the section that follows. A discussion is then presented of the way in which the turbulence is affected by streamline curvature and how the RSTM accounts for these effects. The subsequent section presents the results, and in the final section conclusions are drawn.

Mean Flow Equations

We have the incompressible form of the continuity equation

$$\frac{\partial}{\partial x_i}(U_i) = 0 \tag{1}$$

and momentum equation

$$\rho \frac{\partial}{\partial x_j}(U_i U_j) = -\frac{\partial p}{\partial x_i} + \frac{\partial}{\partial x_j}\left(\mu \frac{\partial U_i}{\partial x_j} - \rho \overline{u_i u_j}\right) \tag{2}$$

Numerical Method. The finite volume computer program CALC-BFC (Boundary Fitted Coordinates) for three-dimensional complex geometries (Davidson and Farhanieh, 1992; Johansson et al., 1993) is used in this study. The program uses Cartesian velocity components, and the pressure-velocity coupling is handled with the SIMPLEC procedure. Staggered grids for the velocities have been used (Patankar, 1980) in most finite volume programs. In the present work, however, a collocated grid arrangement is used, which means that velocities are stored together with the other variables (p, k, ϵ, $\overline{u_i u_j}$) at the center of the control volume. This concept was suggested by Rhie and Chow (1984), and has also been used by, e.g., Burns and Wilkes (1986), Perić et al. (1988), and Majumdar et al. (1992).

The convective terms in the mean flow equations are discretized using QUICK, a third-order scheme by Leonard (1979). For turbulent quantities ($\overline{u^2}$, $\overline{v^2}$, $\overline{uv}$, k, and ϵ) MUSCL, a second-order, bounded scheme of van Leer (1979), is used.

Boundary Conditions. All variables are set to zero at the walls except for pressure, for which $\partial^2 p/\partial n^2 = 0$ is used. At the farfield the velocity components are set from experimental data, i.e.,

$$U = \cos\alpha, \quad V = \sin\alpha, \tag{3}$$

where α denotes angle of attack. The pressure is set from $\partial^2 p/\partial n^2 = 0$. All turbulent quantities are either set to zero or are extrapolated, depending on whether the case is inflow or outflow.

The Reynolds Stress Transport Model

The Reynolds Stress Transport Model has the form (Gibson and Younis, 1986):

$$\underbrace{\frac{\partial}{\partial x_k}(\rho U_k \overline{u_i u_j})}_{\text{convection}} = \underbrace{-\rho\overline{u_i u_k}\frac{\partial U_j}{\partial x_k} - \rho\overline{u_j u_k}\frac{\partial U_i}{\partial x_k}}_{\text{production } P_{ij}} + \Phi_{ij} + D_{ij} - \rho\epsilon_{ij} \tag{4}$$

The convection and production terms are exact and do not require any modelling assumptions. The pressure strain Φ_{ij} and the dissipation ϵ_{ij} are modeled in a standard manner (Gibson and Younis, 1986).

The diffusion term D_{ij} can be modelled using the Generalized Gradient Diffusion Hypothesis GGDH (Daly and Harlow, 1970)

$$D_{ij} = \frac{\partial}{\partial x_m}\left(c_s \rho \overline{u_i u_m}\frac{k}{\epsilon}\frac{\partial \overline{u_i u_j}}{\partial x_k}\right) \tag{5}$$

However, as severe convergence problems were experienced using the GGDH owing to the destabilising cross-derivatives, the diffusion term D_{ij} is modelled using the eddy viscosity assumption

$$D_{ij} = \frac{\partial}{\partial x_m}\left(\frac{\mu_t}{\sigma_t}\frac{\partial \overline{u_i u_j}}{\partial x_m}\right). \tag{6}$$

Following a suggestion by Lien (1992), the turbulent Prandtl number σ_t has been modified. The diffusion in the normal direction is usually much more important than in the streamwise direction. The diffusion coefficient using the eddy viscosity formulation in Eq. (6) is μ_t/σ_t and can be compared with the one in the GGDH-expression in Eq. 5, so that

$$\frac{\nu_t}{\sigma_t} \equiv \frac{c_\mu k^2}{\epsilon\sigma_t} = c_s \frac{k\overline{v^2}}{\epsilon} \tag{7}$$

With $c_s = 0.22$ and $\overline{v^2}/k = 0.5$, we get $\sigma_t = 0.82$. Thus the viscosity in the diffusion term in Eq. (6) is computed as

$$\frac{\mu_t}{\sigma_t} = \frac{\rho}{0.82}\frac{c_\mu k^2}{\epsilon} \tag{8}$$

For ϵ, we obtain the Prandtl number $\sigma_\epsilon = 1$ with $c_\epsilon = 0.18$.

The one-equation eddy viscosity model by Wolfshtein (1969), modified by Chen and Patel (1988), is used near the walls. In this model, the standard k equation is solved and the turbulent length scale is taken from an algebraic expression; for more details see Davidson (1993b).

The k and ϵ-Equations In an RSTM, there are two equivalent sets of equations which can be solved, either $\overline{u^2}$, $\overline{v^2}$, $\overline{w^2}$, $\overline{uv}$, and ϵ or $\overline{u^2}$, $\overline{v^2}$, k, $\overline{uv}$, and ϵ. The latter set has been chosen in the present study. The primary reason for this choice is that the k equation must in any case be solved in the one-equation region.

The standard k and ϵ equations in the RSTM have the form:

$$\frac{\partial}{\partial x_j}(\rho U_j k) = D^k + P^k - \rho\epsilon \tag{9}$$

$$\frac{\partial}{\partial x_j}(\rho U_j \epsilon) = D^\epsilon + \frac{\epsilon}{k}(c_{1\epsilon}P^k - c_{2\epsilon}\rho\epsilon) \tag{10}$$

As for the Reynolds stresses, the diffusion terms D^k, D^ϵ are calculated using the eddy viscosity assumption with $\sigma_k = 0.82$ and $\sigma_\epsilon = 1$, see Eqs. (6)–(8).

Two Variants of RSTM. Two different Reynolds stress models are compared. One is the standard model of Gibson and Launder (1978) (hereafter denoted GL), which has been used extensively in the literature. The other model is that proposed by Gibson and Younis (1986) (hereafter denoted GY). The two models differ only in the choice of constants. When modelling the pressure strain term $\Phi_{ij,1} + \Phi_{ij,2}$, there are three chief physical processes used to determine the constants: (*a*) return-to-isotropy when all mean strains are zero, (*b*) rapid-distortion theory, and (*c*) experimental stress levels in simple shear flows. In the GL model, (*b*) and (*c*) have been favoured at the expense of (*a*). Lumley (1978) argues that (*b*) is not relevant since it is assumed in rapid-distortion theory that the mean strain (the rapid part of the pressure-strain term, $\Phi_{ij,2}$) acts on the entire turbulence spectra. In reality, it acts only on the low-wave number part of the spectra, i.e., the large scales, whose energy is spread to the smaller scales through the cascade effect. In the GY model, the criteria dictated by rapid distortion is relaxed, and the return-to-isotropy criterion is taken fully into account. The constants for the two models are:

Model GY (c_1, c_2, c_1', c'_2, $c_{1\epsilon}$, $c_{2\epsilon}$) = (3.0, 0.3, 0.75, 0.15, 1.4, 1.8)

Model GL (c_1, c_2, c_1', c_2', $c_{1\epsilon}$, $c_{2\epsilon}$) = (1.8, 0.6, 0.5, 0.3, 1.44, 1.9)

The two models are compared in Fig. 1. Model GY is otherwise used throughout this study.

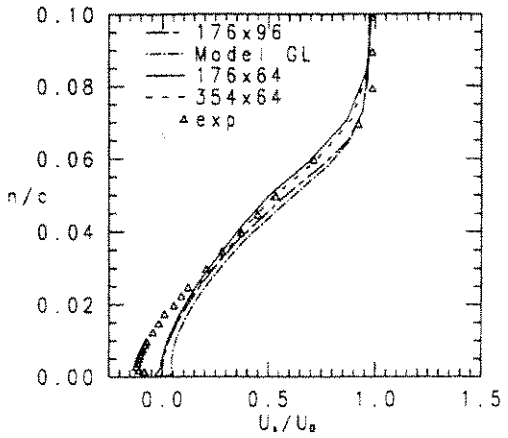

Fig. 1 U_s profiles predicted with RSTM (Model GY) using different meshes. The U_s profile computed with Model GL is also included (mesh 176 × 96)

Streamline Curvature

When the streamlines in boundary layer flow have a convex curvature, the turbulence is stabilised. This dampens the turbulence (Bradshaw, 1973; Rodi and Scheuerer, 1983), especially the shear stress and the Reynolds stress normal to the wall. Concave curvature destabilises the turbulence. The ratio of boundary layer thickness δ to curvature radius R is a common parameter for quantifying the curvature effects on the turbulence. The work reviewed by Bradshaw demonstrates that even such small amounts of convex curvature as $\delta/R = 0.01$ can have a significant effect on the turbulence. Thompson and Whitelaw (1985) carried out an experimental investigation on a configuration simulating the flow near a trailing edge of an airfoil, where they measured $\delta/R = 0.03$. They reported a 50 percent decrease of $\rho\overline{v^2}$ (Reynolds stress in the normal direction to the wall) owing to curvature. The reduction of $\rho\overline{v^2}$ and $-\rho\overline{uv}$ was also substantial. In addition, they reported significant damping of the turbulence in the shear layer in the outer part of the separation region.

An illustrative model case is curved boundary layer flow. A polar coordinate system $r - \theta$ with θ locally aligned with the streamline is introduced. As $U_\theta = U_\theta(r)$ (with $\partial U_\theta/\partial r > 0$ and $U_r = 0$), the radial inviscid momentum equation degenerates to

$$\frac{\rho U_\theta^2}{r} - \frac{\partial p}{\partial r} = 0 \tag{11}$$

Here the variables are instantaneous or laminar. The centrifugal force exerts a force in the normal direction (outward) on a fluid following the streamline, which is balanced by the pressure gradient. If the fluid is displaced by some disturbance (e.g., turbulent fluctuation) outwards to level A, it encounters a pressure gradient larger than that to which it was accustomed at $r = r_0$, as $(U_\theta)_A > (U_\theta)_0$, which from Eq. (11) gives $(\partial p/\partial r)_A > (\partial p/\partial r)_0$. Hence the fluid is forced back to $r = r_0$. Similarly, if the fluid is displaced inwards to level B, the pressure gradient is smaller here than at $r = r_0$ and cannot keep the fluid at level B. Instead the centrifugal force drives it back to its original level.

It is clear from the model problem above that convex curvature, when $\partial U_\theta/\partial r > 0$, has a stabilizing effect on (turbulent) fluctuations, at least in the radial direction. It is discussed below how the Reynolds stress model responds to streamline curvature.

Assume that there is a flat-plate boundary layer flow. The ratio of the normal stresses $\rho\overline{u^2}$ and $\rho\overline{v^2}$ is typically 5. At one x station, the flow is deflected upwards. How will this affect the turbulence? Let us study the effect of concave streamline curvature. The production terms P_{ij} in Eq. (4) owing to rotational strains can be written as

Table 1 Effect of streamline curvature on turbulence

	$\partial U_\theta/\partial r > 0$	$\partial U_\theta/\partial r < 0$
Convex curvature	stabilizing	destabilizing
Concave curvature	destabilizing	stabilizing

$$\text{RSTM, } \overline{u^2}\text{ – eq. : } \quad P_{11} = -2\rho\overline{uv}\frac{\partial U}{\partial y} \tag{12}$$

$$\text{RSTM, } \overline{uv}\text{ – eq. : } \quad P_{12} = -\rho\overline{u^2}\frac{\partial V}{\partial x} - \rho\overline{v^2}\frac{\partial U}{\partial y} \tag{13}$$

$$\text{RSTM, } \overline{v^2}\text{ – eq. : } \quad P_{22} = -2\rho\overline{uv}\frac{\partial V}{\partial x} \tag{14}$$

$$k - \epsilon : P^k = \mu_t\left(\frac{\partial U}{\partial y} + \frac{\partial V}{\partial x}\right)^2 \tag{15}$$

As long as the streamlines are parallel to the wall, all production is a result of $\partial U/\partial y$. However as soon as the streamlines are deflected, there are more terms resulting from $\partial V/\partial x$. Even if $\partial V/\partial x$ is much smaller than $\partial U/\partial y$ it will still contribute non-negligibly to P_{12} as $\rho\overline{u^2}$ is much larger than $\rho\overline{v^2}$. Thus the magnitude of P_{12} will increase (P_{12} is negative) as $\partial V/\partial x > 0$. An increase in the magnitude of P_{12} will increase $-\overline{uv}$, which in turn will increase P_{11} and P_{22}. This means that $\rho\overline{u^2}$ and $\rho\overline{v^2}$ will be larger and the magnitude of P_{12} will be further increased, and so on. It is seen that there is a positive feedback, which continuously increases the Reynolds stresses. It can be said that the turbulence is destabilised owing to concave curvature of the streamlines.

However, the $k - \epsilon$ model is not very sensitive to streamline curvature (neither convex nor concave), as the two rotational strains are multiplied by the same coefficient (the turbulent viscosity).

If the flow (concave curvature) is a wall jet flow where $\partial U/\partial y < 0$, the situation will be reversed: the turbulence will be stabilised. If the streamline (and the wall) is deflected downwards, the situation will be as follows: the turbulence is stabilizing when $\partial U/\partial y > 0$, and destabilizing for $\partial U/\partial y < 0$.

The stabilising or destabilising effect of streamline curvature is thus dependent on the type of curvature (convex or concave), and whether there is an increase or decrease in momentum in the tangential direction with radial distance from its origin (i.e., the sign of $\partial U_\theta/\partial r$). For convenience, these cases are summarized in Table 1.

Results

The results calculated are compared with experimental data taken from Capbern and Bonnet (1989) and Gleyzes (1989). The experimental airfoil is the A-profile, which also was used in the CFD validation EUROVAL project (1993). The Reynolds number and the Mach number are 2.1×10^6 and 0.15, respectively. In the calculations, the flow is assumed to be incompressible. Measurements have been carried out in two wind tunnels, F1 and F2, the F1 wind tunnel being larger than F2. Global characteristics such as friction coefficients and surface pressures were measured in the F1 wind tunnel, whereas the flow field was studied in more detail in the F2 wind tunnel where mean velocity profiles and Reynolds stresses were measured using a three-component LDV system. The blockage effect in the F2 tunnel was more important than in the F1 tunnel, leading to three-dimensional effects for $\alpha \geq 13$ deg.

The Mesh. A C-mesh with 353 × 65, generated by Chanez and Palicot (1990), was used. The near-wall nodes are located at $y^+ \simeq 1$, and 7 to 10 nodes—in the normal direc-

tion—are situated in the region $0 \leq y^+ \leq 20$. Two modifications of this mesh have been tested. In the first modification the number of nodes in the tangential direction to the airfoil was divided by two (178 × 65). In these two meshes a constant stretching factor in the normal direction was used. In the second modification of the 353 × 65 mesh, the stretching factor was decreased from 1.12 to 1.07 between $n/c = 0.0029$ and $n/c = 0.12$, adding 32 extra nodes in the boundary layer so that a 178 × 96 node mesh was obtained.

The thickness of the experimental (real) airfoil is finite at the trailing edge, whereas it is preferable in the calculations that it is zero. Following the procedure chosen in EUROVAL, the lower surface near the trailing edge is displaced slightly upwards so that it joins the upper surface at $x/c = 1.0$, thus giving the same airfoil length as in the experiments.

Transition. Transition was initially imposed by setting k, ϵ, $\overline{u^2}$, $\overline{v^2}$, $\overline{uv}$ to zero before the transition point. After the transition point the turbulence quantities grow naturally without any sort of triggering. The reason why no triggering is needed is because of the one-equation model, which does not damp the turbulent as much as other low-Re models. In an earlier work (Davidson, 1990), where the low-Re model of Chien (1982) was used, is was found necessary to introduce some turbulence after the transition point.

Setting the turbulent quantities to zero before the transition point, created some problems on the 353 × 65, which resulted in separation on the suction side of the airfoil where the transition was imposed, probably because it caused too abrupt an increase in the viscosity. Thus the transition is imposed more smoothly, which is probably also more physically correct. If the transition is to be imposed at x_{tr}, the turbulent viscosity is made to vary linearly in the x direction between its calculated values at $x_{tr} - \Delta x$ and x_{tr}; for $\alpha = 13.3$ deg, on the upper side, $x_{tr}/c = 0.12$, $\Delta x/c = 0.05$ were used, and on the lower side $x_{tr}/c = 0.3$, $\Delta x/c = 0$ were used.

Mean Flow Quantities. The velocity profiles at $x/c = 0.96$ are presented in Fig. 1 using the three different meshes. It can be seen that the doubling of the number of mesh points in the tangential direction to the airfoil does not have any great effect on the calculated results. Included in Fig. 1 is also the velocity profile predicted with the Model GL, a profile which is more smeared out compared with Model GY, which means that the former model predicts a more diffusive (turbulent) flow field with larger Reynolds stresses. It is instructive to study the truncated ASM (Rodi, 1980) form of the stress tensor

$$\overline{u_i u_j} = \frac{2}{3}\delta_{ij}k + \frac{k}{\epsilon}\frac{(1-c_2)\left(P_{ij} - \frac{2}{3}\delta_{ij}P^k\right) + \Phi'_{ij,1} + \Phi'_{ij,2}}{c_1 - 1 + P^k/\epsilon} \tag{16}$$

On the curved part of the airfoil (close to the wall) up to approximately mid-chord, as well as close to the wall in the separation region, the dissipation is larger than P^k, i.e., $P^k/\epsilon < 1$ (see Fig. 10). The denominator in Eq. (16) is reduced as its last term decreases, which augments $\overline{u_i u_j}$. As the coefficient c_1 has the value 1.8 in Model GL compared with 3.0 in Model GY, the relative importance of P^k/ϵ is larger for Model GL; the resulting increase in $\overline{u_i u_j}$ with Model GL gives a more smeared out velocity profile and counteracts the streamline curvature-induced reduction resulting from convex curvature. All results presented below have been obtained using the 178 × 96 mesh and Model GY.

In Fig. 2 the RSTM-predicted lift-coefficients C_L are compared with two-layer $k - \epsilon$ predictions and experimental data. It can be seen that the RSTM agrees well with experiments predicting decreasing C_L at $\alpha = 17$ deg, which agrees well with experimental data. However, the $k - \epsilon$ model shows no tendency to predict stall. It should be noted that there is a considerable difference between the experimental results in the two wind tunnels F1 and F2. The results obtained in the larger wind tunnel F1, are considered to be more reliable than those obtained in F2. This should be kept in mind when making detailed comparisons between experimental profiles taken in F2 and calculated results.

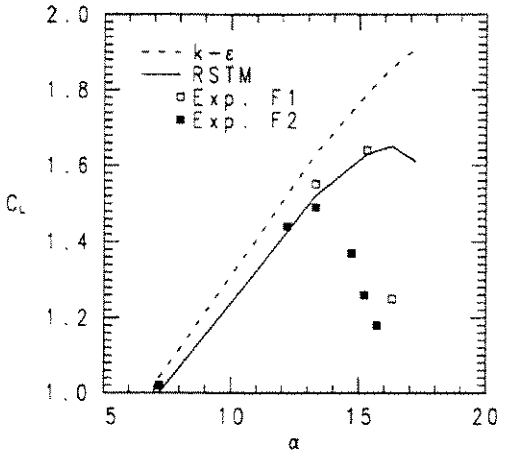

Fig. 2 Lift-coefficients C_L versus angle of attack α

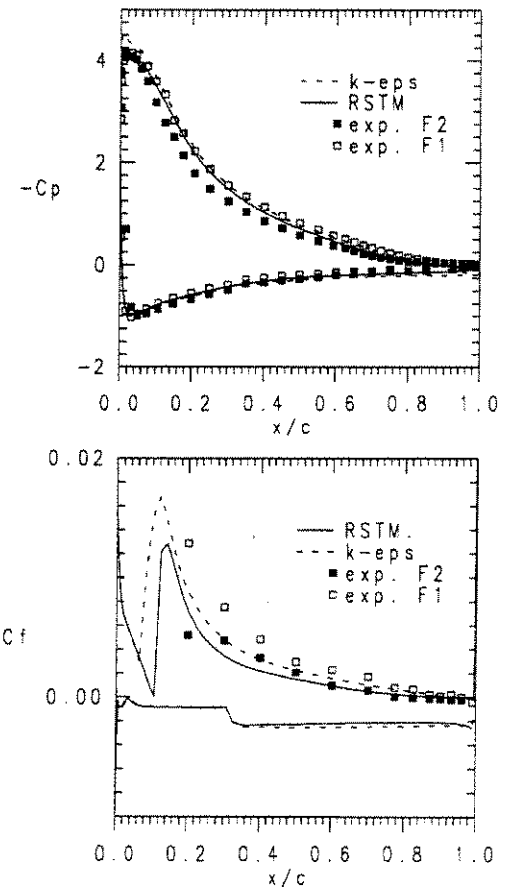

Fig. 3 Wall pressure $c_p = (p - p_0)/0.5\rho U_0^2$ and skin friction $\tau_w/1/2\rho U_0^2$

The wall pressure and the skin friction are presented in Fig. 3. It can be seen that, with the $k - \epsilon$ model, the (negative) pressure peak at the suction side is overpredicted as compared with experiments, and that the RSTM predictions agree well with experiments. The skin friction predicted with $k - \epsilon$ is higher than that predicted with RSTM. This is probably partly due to how the models react to the imposed transition, but it

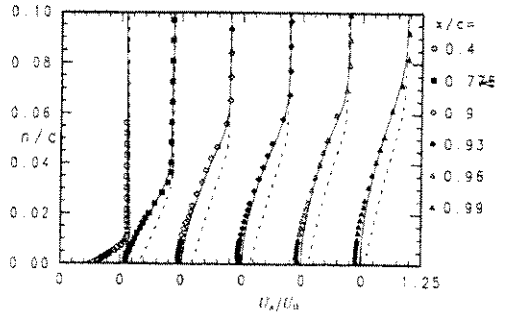

Fig. 4 U_s profiles on the suction side of the airfoil. Solid lines: RSTM; dashed lines: $k - \epsilon$

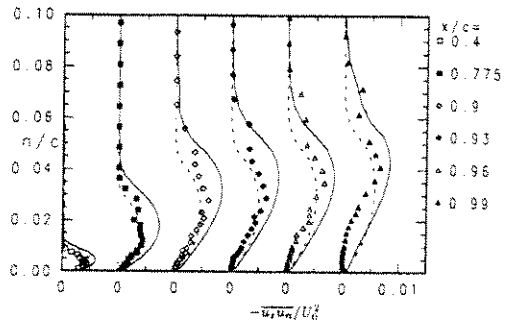

Fig. 6 $\overline{u_s u_n}$ profiles on the suction side of the airfoil. Solid lines: RSTM; dashed lines: $k - \epsilon$

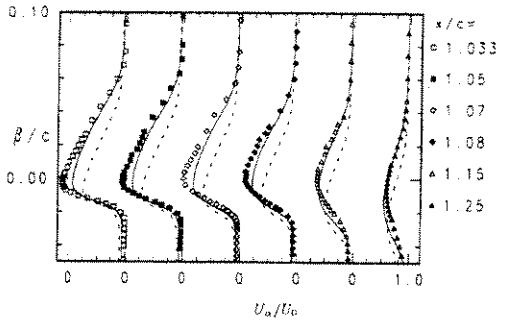

Fig. 5 U_α profiles in the wake after the airfoil. Solid lines: RSTM; dashed lines: $k - \epsilon$

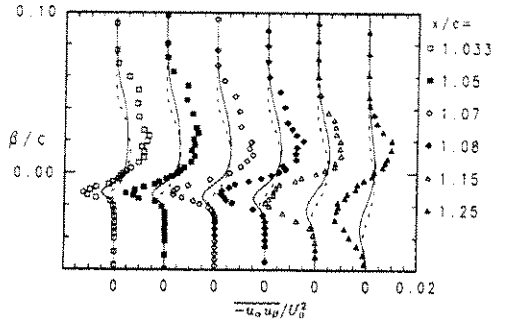

Fig. 7 $\overline{u_\alpha u_\beta}$ profiles in the wake after the airfoil. Solid lines: RSTM; dashed lines: $k - \epsilon$

is also logical since the velocity profiles (see below) predicted with the RSTM show more tendency to separate than do the $k - \epsilon$ profiles. But it was also found in a previous work on testing different low-Re variants of $k - \epsilon$ models (Davidson, 1993a), that predicted skin-frictions are not a very reliable indicator of the global flow characteristics, not even the velocity profiles.

The velocity profiles on the suction side of the airfoil are presented in Fig. 4. Note that an orthogonal $s - n$ coordinate system is used, with origin on the surface. The s coordinate is tangential to the airfoil. The U_s-velocities on the airfoil are well predicted when using the RSTM. A small separation is predicted, occurring at $x/c = 0.90$. This type of separation can be termed *incipient detachment* (Simpson, 1989). As separation is approached, it is seen that the predicted U_s profiles follow the experimental ones, that the profiles become progressively less full and that an inflexion point appears in the profiles. The separation region in the experiments is considerably larger than that in the RSTM-predictions. This may perhaps be attributed to experimental uncertainty in the F2 wind tunnel, because the lift-coefficient in Fig. 2 and the surface pressure data in Fig. 3 indicate that the separation zone in the more reliable measurements in the F1 wind tunnel is smaller. The velocity profiles predicted with the $k - \epsilon$ model do not agree very well with experiments: no tendency toward separation is observed, which implies that the $k - \epsilon$ predicts excessively large shear stresses, giving too high a turbulent diffusion and thus smearing out the U_s profiles.

The wake velocity profiles U_α/U_0 are compared with experiments in Fig. 5. Note that an $\alpha - \beta$ coordinate system is used in the wake with origin at the trailing edge; the α axis is parallel to the free-stream velocity, and β is orthogonal to α. From Fig. 5 it can be seen that the RSTM shows better performance than the $k - \epsilon$ model.

Turbulent Quantities. The stresses on the airfoil and the wake are presented in Figs. 6–7. Using RSTM, the shear stresses are in fairly good agreement with experimental data, whereas the shear stresses are overpredicted, especially near the trailing edge. In the wake, the predicted shear stresses are much smaller than in the experiments, which is probably related to the larger experimental separation zone.

The shear stresses predicted with the $k - \epsilon$ model are smaller than those predicted with the RSTM. The reason why the shear stresses are higher with RSTM than with $k - \epsilon$ is that the turbulent quantities were computed with different velocity fields. The velocity gradients in the $k - \epsilon$ predictions are smaller than in the RSTM predictions, leading to lower production of turbulence in the former case.

When presenting turbulent quantities such as Reynolds stresses, it may be overlooked that it is not the stresses that enter the momentum equations but their gradients, where the Reynolds stresses constitute net (vectorial) forces/area, i.e., net stress vectors. The force resulting from shear stresses, $\mathbf{F}_s$ can be written

$$\mathbf{F}_s = \rho\left(-\frac{\partial\overline{uv}}{\partial x}, \quad -\frac{\partial\overline{uv}}{\partial y}\right), \tag{17}$$

and from the normal stresses:

$$\mathbf{F}_n = \rho\left(-\frac{\partial\overline{u^2}}{\partial x}, \quad -\frac{\partial\overline{v^2}}{\partial y}\right), \tag{18}$$

which should be compared to the force resulting from pressure

$$\mathbf{F}_p = \left(-\frac{\partial p}{\partial x}, \quad -\frac{\partial p}{\partial y}\right) \tag{19}$$

In Fig. 8, the force-fields near the trailing edge are presented as vector plots. It can be seen from the pressure force F_p that the flow goes against an adverse pressure gradient, both on the suction side of the airfoil and in the wake. It is interesting to see how the forces (net stress vectors) resulting from the Reynolds stresses are fairly important in the wake region, especially along the centre line, where the very thin boundary layer from the pressure side mixes with the separated boundary layer from the suction side. Large gradients are formed that give strong

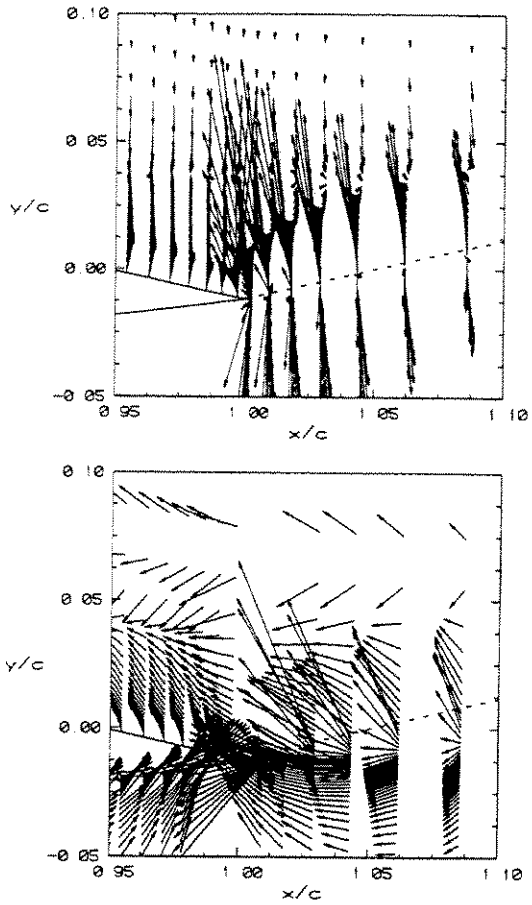

Fig. 8 Vector plots of turbulent stresses and pressure vectors near the trailing edge. The same scaling of vectors is used in all plots. The dashed line has the same direction as the far-field flow (α = 13.3). (*a*) $\rho(-\overline{\partial uv/\partial x}, -\overline{\partial uv/\partial y})$, (*b*) $(-\partial p/\partial x, -\partial p/\partial y)$

downward forces owing to both shear and normal stresses (the normal stresses are not shown here due to space constraints; see Davidson, 1993c), which are even larger than the forces resulting from the pressure gradient.

As Cartesian velocity components have been used in the calculations, no explicit curvature terms appear in the Reynolds stress equations (see Eq. (4)). Of course, the Reynolds stresses formulated in Cartesian coordinates are also affected by curvature, but are affected *implicitly*. To investigate the curvature effects, let us—in the post-processing—study the equations in polar coordinates $r - \theta$, with the flow in the circumferential θ direction (i.e., $U_\theta = U_\theta(r)$, $U_r = 0$). The θ axis is thus chosen so that the flow is locally aligned with this axis. Curvature terms now appear because the r = const. coordinate lines are curved. The Reynolds stress equation can, in symbolic form, be written

$$C_{ij} - D_{ij} = P_{ij} + \Phi_{ij} - \epsilon_{ij} + P^c_{ij} + C^c_{ij} \qquad (20)$$

where superscript c on P_{ij} and C_{ij} denotes curvature terms originating from production and convection, respectively, see Table 1. The larger these terms, the more important the curvature effects.

The flux Richardson number

$$R_f = \frac{2U_\theta/r}{U_\theta/r + \partial U_\theta/\partial r} \qquad (21)$$

is a convenient parameter for studying curvature effects. Its physical meaning is (minus) the ratio of the production of $\overline{u_r^2}$ owing to curvature to the total production of $\overline{u_\theta^2}$ (see Table 2). The ratio δ/R and the flux Richardson number are shown in Fig. 9 at three different x stations: at x/c = 0.2 where the wall

Table 2 Source terms in the Reynolds stress equations (see Eq. (20)) due to production and convection in a polar coordinate system

	P_{ij}	P^c_{ij}	C^c_{ij}
$\overline{u_r^2}$	—	$2\overline{u_r u_\theta}\dfrac{U_\theta}{r}$	$2\overline{u_r u_\theta}\dfrac{U_\theta}{r}$
$\overline{u_\theta^2}$	$-2\overline{u_r u_\theta}\dfrac{\partial U_\theta}{\partial r}$	—	$-2\overline{u_r u_\theta}\dfrac{U_\theta}{r}$
$\overline{u_r u_\theta}$	$-\overline{u_r^2}\dfrac{\partial U_\theta}{\partial r}$	$\overline{u_\theta^2}\dfrac{U_\theta}{r}$	$(\overline{u_\theta^2} - \overline{u_r^2})\dfrac{U_\theta}{r}$

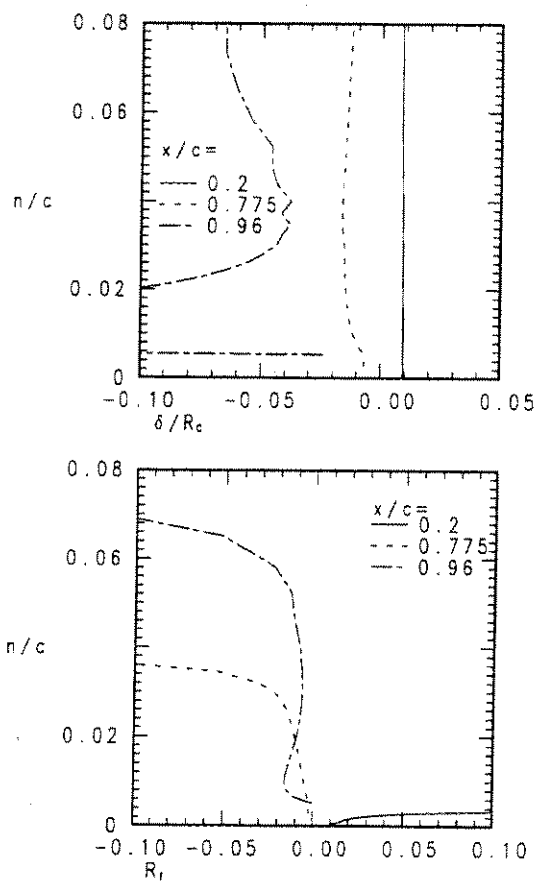

Fig. 9 Parameters describing streamline curvature effects on the turbulence. (*a*) Boundary layer thickness over streamline curvature radius δ/R_c. (*b*) Flux Richardson number R_f

curvature is most important, near the separation point (x/c = 0.775) and in the separation zone (x/c = 0.96). As can be seen, the streamline curvature is positive at x/c = 0.2, which in the outer part of the boundary layer gives an increasing flux Richardson number. The flow here is parallel to the curved wall, which gives constant $\delta/R_c \approx 0.01$, i.e. boundary thickness over wall curvature. The boundary layer is very thin ($\delta/c \approx 0.005$), which explains the strong increase in the flux Richardson number at $n/c \approx 0.004$, close to the outer edge of the boundary layer. As separation is approached, the streamlines become concave, which destabilises the turbulence. It is seen in Fig. 9 that δ/R and R_f become negative. The flux Richardson number reaches values of ± 0.1 in the outer region of the boundary layer. These values should be compared with reported values on the critical flux Richardson number (the R_f-value at which the turbulence collapse, suppressed by dissipation and buoyancy/curvature effects) in buoyant flows, ranging between 0.15 (Ellison, 1957) and 0.5 (Townsend, 1958). The curvature effects are largest in the outer boundary layer, where the curvature term U_θ/R becomes comparable with

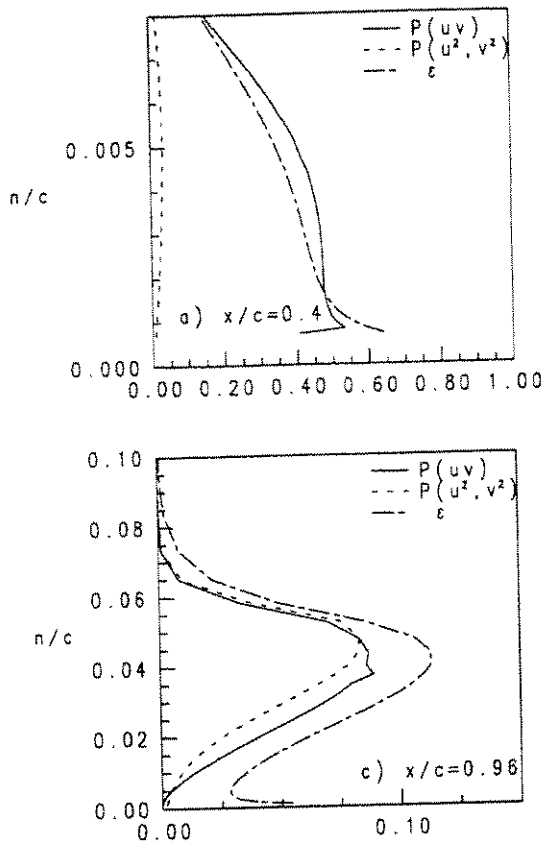

Fig. 10 Calculated productions terms in the k equation. Solid lines: $-\overline{u_s u_n}\,\partial U_s/\partial n$; dashed lines: $(\overline{u_n^2}-\overline{u_s^2})\partial U_s/\partial s$; dashed-dotted lines: ϵ. (a) x/c = 0.4, (b) x/c = 0.96

the velocity gradient $\partial U_\theta/\partial r$. The direct influence of the curvature effects are thus largest in the outer part of the boundary layer, but they will also have indirect influence via convective and diffusive transport. The Reynolds stresses, augmented or dampened by curvature, increase or decrease the production terms in the equations and, through convection and diffusion, also affect the surroundings.

The streamlines bounding the separation region in separated flows are usually convex. It may be noted that, in the present case, the turbulence in the shear layer bounding the separation zone on the suction side is mostly destabilised as a result of the concave curvature of the streamlines. This is because the flow is forced upwards when it reaches the wake, giving concave streamline curvature in the region of the trailing edge.

The production contribution to the k-equation from the shear stress $-\overline{u_s u_n}\partial U_s/\partial n$ and the normal stresses $-(\overline{u_s^2}-\overline{u_n^2})\partial U_s/\partial s$ are presented in Fig. 10. The production resulting from the normal stresses is not very large at x/c = 0.4 (at most, ten percent of that resulting from the shear stress). Near the separation point (the conditions near the separation point are not shown here due to space constraints; see Davidson, 1993c) and in the separation region, the two terms are of equal importance. The dissipation is also presented in Fig. 10, and it is seen that production and dissipation balance each other at x/c = 0.4, but that this is not the case near the separation point or in the separation region.

Conclusions

The flow around a low-speed airfoil has been computed. The code used is based on SIMPLEC, which employs collocated grid arrangement and solves for the Cartesian velocities. A third-order differencing scheme (QUICK) for the mean flow equations has been used together with a second-order, bounded scheme (MUSCL) for the turbulent quantities. Two turbulence models are compared: a Reynolds Stress Transport Model (RSTM) and a $k-\epsilon$ model. As neither model is valid in the viscous-dominated near-wal region, they are matched with a one-equation eddy-viscosity model.

The most important global feature of a low-speed airfoil is to determine at which angle of attack stall occurs. In the present work, it has been shown that an adequate turbulence model should be used, capable of accounting for important physical phenomena such as transport of individual stresses, streamline curvature effects and irrotational strains. In order to account for these effects, the turbulence model must properly respond to irrotational strains and the interaction process between strains and all Reynolds stresses. The only model that fulfills these requirements is a Reynolds Stress Transport Model (or perhaps its algebraic variant, ASM).

The following conclusions can be drawn.

- The RSTM predicts the flow in good agreement with experimental data, and a small separation zone is predicted at α = 13.3 deg which could be described as incipient detachment. The computed lift coefficient C_L has a maximum at an angle of attack of 17 deg, indicating approaching stall, which is in good agreement with experimental data.
- The $k-\epsilon$ model predictions are in poor agreement with experiments, the computed flow showing no tendency toward separation at α = 13.3 deg. No stall is predicted and the lift coefficient continues to increase at α = 17 deg.
- Curvature effects resulting from wall curvature and streamline curvature are important. Computed curvature radii show that the boundary layer thickness over curvature radius is approximately 0.01 (δ/R_C = 0.01) at the suction side close to the pressure minimum. In the region in which the flow approaches the separation region, it is forced further away from the wall. This results in streamlines with a concave curvature; values of δ/R_C close to -0.05 are found.
- When comparing Reynolds stresses one may overlook it is not the Reynolds stresses that appear in the momentum equations but their gradients. The (net) stress vectors resulting from shear stresses $\rho(-\partial\overline{uv}/\partial x, -\partial uv/\partial y)$ and normal stresses $\rho(-\partial\overline{u^2}/\partial x, -\partial\overline{v^2}/\partial y)$ are compared with the forces (per unit volume) resulting from the pressure gradient $(-\partial p/\partial x, -\partial p/\partial y)$ in the region of the trailing edge. It is found that the forces that results from both normal stresses and shear stresses are comparable to the forces resulting from the pressure gradient.
- Two variants of RSTM have been tested: the model of Gibson and Launder (1978) (GL), which is the "standard" one, and the model of Gibson and Younis (1986) (GY). The difference between the models lies in the choice of constants. It was found that the Model GL is more diffusive than Model GY, the reason being that the ratio P^k/ϵ is smaller than one, which has a greater effect in the former model in which the c_1-coefficient has a smaller value (c_1 = 1.8) than in Model GY (c_1 = 3.0). In the present work, Model GY has been used throughout the study, as this model gave better agreement with experiments than Model GL.

References

Bradshaw, P., 1973, "Effects of Streamline Curvature on Turbulent Flow," AGARDograph, no. 169.

Burns, A. D., and Wilkes, N. S., 1986, "A Finite Difference Method for the Computation of Fluid Flow in Complex Three-Dimensional Geometries," Report AERE R 12342, Harwell Laboratory, U.K..

Capbern, C., and Bonnet, C., 1989, "Opération décrochage: Rapport Final de Synthèse," Report Aerospatiale 443.535./89, Toulouse.

Cebeci, T., 1989, "Essential Ingredients of a Method for Low Reynolds-Number Airfoils," *AIAA Journal*, Vol. 27, pp. 1680–1688.

Chanez, Ph. and Palicot, L., 1990, "Évaluation d'un code Navier-Stokes

bidimensionnel pour le calcul de l'écoulement autour d'un profil d'aile," Report Aerospatiale, 443.548/90, Toulouse.

Chen, H. C. and Patel, V. C., 1987, "Practical Near-Wall Turbulence Models for Complex Flows Including Separation," *AIAA J.*, Vol. 26, pp. 641–648.

Chien, K. Y., 1982, "Predictions of Channel and Boundary Layer Flows with a Low-Reynolds Number Turbulence Model," *AIAA Journal*, Vol. 20, pp. 33–38.

Daly, B. J. and Harlow, F. H., 1970, "Transport Equations of Turbulence," *Physics of Fluids*, Vol. 13, pp. 2634–2649.

Davidson, L., 1990, "Implementation of a Semi-Implicit $\kappa - \epsilon$ Turbulence Model in a Explicit Runge-Kutta Navier-Strokes Code," Report TR/RF/90/25, CERFACS, Toulouse.

Davidson, L. and Farhanieh, B., 1992, "CALC-BFC: A Finite-Volume Code Employing Collocated Variable Arrangement and Cartesian Velocity Components for Computation of Fluid Flow and Heat Transfer in Complex Three-Dimensional Geometries," Report 92/4, Thermo and Fluid Dynamics, Chalmers University of Technology, Gothenburg.

Davidson, L. and Rizzi, A., 1992, "Navier-Stokes Stall Predictions Using an Algebraic Stress Model," *Journal of Spacecraft and Rockets*, Vol. 29, pp. 794–800 (see also AIAA-paper 92–0195, Reno, Jan. 1992).

Davidson, L., 1993a, "CERFACS' contribution in Task 3.2 to EUROVAL: A European Initiative on Validation of CFD-codes," W. Haase, F. Brandsma, E. Elsholz, M. Leschziner and D. Schwamborn, (eds.), Notes on Numerical Fluid Mechanics, Vol. 42, Vieweg Verlag.

Davidson, L., 1993b, "Reynolds Stress Transport Modelling of Shock/Boundary-Layer Interaction," AIAA-paper 93–2936, AIAA 24th Fluid Dynamics Conference, Orlando, July.

Davidson, L., 1993c, "High-Lift Airfoil Flow Simulations Using a Two-Layer Reynolds Stress Transport Model," Proc *5th International Symposium on Refined Flow Modelling and Turbulence Measurements*, pp. 777–784, Paris, Sept. 7–10.

Ellison, T. H., 1957, "Turbulent Transport of Heat and Momentum From an Infinite Rough Plane," *Journal of Fluid Mechanics*, Vol. 2, pp. 456–466.

Euroval, 1993, "A European Initiative on Validation of CFD-codes," W. Haase, F. Brandsma, E. Elsholz, M. Leschziner and D. Schwamborn, (eds.), *Notes on Numerical Fluid Mechanics*, Vol. 42, Vieweg Verlag.

Gibson, M. M. and Launder, B. E., 1978, "Ground Effects on Pressure Fluctuations in the Atmospheric Boundary Layer," *Journal of Fluid Mechanics*, Vol. 86, pp. 491–512.

Gibson, M. M. and Younis, B. A., 1986, "Calculation of Swirling Jets With a Reynolds Stress Closure," *Physics of Fluids*, Vol. 29, pp. 38–48.

Gleyzes, C., 1989, "Opération décrochage: Résultats de la deuxième campagne d'essais à F2 (mesures de pression et vélocimetrie laser)," Report ONERA/CERT 57/5004.22, Toulouse.

Johansson, S., Davidson, L. and Olsson, E., 1993, "Numerical Simulation of Vortex Shedding Past Triangular Cylinders at High Reynolds Number," *International Journal for Numerical Methods in Fluids*, Vol. 16, pp. 859–878.

Leonard, B. P., 1979, "A Stable and Accurate Convective Modelling Based on Quadratic Upstream Interpolation," *Computational Methods in Applied Mechanical Engineering*, Vol. 19, pp. 59–98.

Lien, F. S., 1992, "Computational Modelling of 3D Flow in Complex Ducts and Passages," PhD thesis, University of Manchester, Manchester.

Lumley, J. L., 1978, "Computational Modelling of Turbulent Flows," *Advances in Applied Mechanics*, Vol. 18, pp. 123–176.

Majumdar, S., Rodi, W. and Zhu, J., 1992, "Three-Dimensional Finite-Volume Method for Incompressible Flows With Complex Boundaries," ASME JOURNAL OF FLUIDS ENGINEERING, Vol. 114, pp. 496–503.

Patankar, S. V., 1980, Numerical Heat *Transfer and Fluid Flow*, McGraw-Hill, New York.

Rhie, C. M. and Chow, W. L., 1984, "Numerical Study of the Turbulent Flow Past an Airfoil with Trailing Edge Separation," *AIAA Journal*, Vol. 21, pp. 1527–1532.

Perić, M., Kessler, K. and Scheuerer, G., 1988, "Comparison of Finite-Volume Numerical Methods with Staggered and Collocated GRIDS," *Computer & Fluids*, Vol. 16, pp. 389–403.

Rodi, W., 1980, *Turbulence Models and Their Application in Hydraulics*, International Association of Hydraulic Research, Monograph, Delft.

Rodi, W. and Scheuerer, G., 1983, "Calculation of Curved Shear Layers With Two-Equation Turbulence Models," *Physics of Fluids*, Vol. 26, pp. 1422–1435.

Simpson, R. L., 1989, "Turbulent Boundary-Layer Separation," *Annual Review in Fluid Mechanics*, Vol. 21, pp. 205–234.

Thompson, B. E. and Whitelaw, J. H., 1985, "Characteristics of a Trailing-Edge Flow With Turbulent Boundary-Layer Separation," *Journal of Fluid Mechanics*, Vol. 157, pp. 305–326.

Townsend, A. A., 1958, "Turbulent Flow in Stably Stratified Atmosphere," *Journal of Fluid Mechanics*, Vol. 3, pp. 361–372.

Van Leer, B., 1979, "Towards the Ultimate Conservative Difference Scheme. V. A. Second-Order Sequel to Godonov's Method," *Journal of Computational Physics*, Vol. 32, pp. 101–136.

Wolfshtein, M., 1969, "The Velocity and Temperature Distribution in One-Dimensional Flow with Turbulence Augmentation and Pressure Gradient," *International Journal Heat and Mass Transfer*, Vol. 12, pp. 301–318.